Geomechanics and Engineering, *Vol. 15, No. 3 (2018) 811-822*
DOI: https://doi.org/10.12989/gae.2018.15.3.811

Characteristic of size distribution of rock chip produced by rock cutting with a pick cutter

Hoyoung Jeong and Seokwon Jeon*

Department of Energy Systems Engineering, Seoul National University, 1 Gwanak-ro, Gwanak-gu, Seoul 08826, Republic of Korea

(Received May 30, 2017, Revised February 12, 2018, Accepted March 23, 2018)

Abstract. Chip size distribution can be used to evaluate the cutting efficiency and to characterize the cutting behavior of rock during cutting and fragmentation process. In this study, a series of linear cutting tests was performed to investigate the effect of cutting conditions (specifically cut spacing and penetration depth) on the production and size distribution of rock chips. Linyi sandstone from China was used in the linear cutting tests. After each run of linear cutting machine test, the rock chips were collected and their size distribution was analyzed using a sieving test and image processing. Image processing can rapidly and cost-effectively provide useful information of size distribution. Rosin-Rammer distribution pamameters, the coarseness index and the coefficients of uniformity and curvature were determined by image processing for different cutting conditions. The size of the rock chips was greatest at the optimum cut spacing, and the size distribution parameters were highly correlated with cutter forces and specific energy.

Keywords: chip size distribution; image processing; linear cutting machine (LCM) test; pick cutter; rock powder; cutting efficiency

1. Introduction

Mechanical excavation has been widely used in civil and mining projects, and demand for this method is rapidly increasing due to its numerous advantages in terms of safety, stability, high advance rate, less environmental impact and construction practice compared with the drill and blasting method (Jeong *et al.* 2014). Especially, mechanical excavation is sometimes essential for urban and subsea tunneling and subsea trenching.

Various types of mechanical excavators (e.g., tunnel boring machines(TBMs), roadheaders, longwall shearers and trenchers) with mounted cutting tools (e.g., disc cutter, pick cutter and drag bit) can be used to excavate rock mass. Of the machines, partial-face excavation machines generally used a pick cutter as cutting tools (Chang *et al.* 2017). It is important to estimate the cutter forces (i.e., normal, cutting and side forces) that act on cutting tools when cutting a particular type of rock to determine operational parameters (Jeong *et al.* 2016).

The cutters on a cutter-head have a specific spacing, known as cut spacing (or cutter spacing). The cut spacing is an important parameter to determine cutter arrangement and the number of cutters on a cutter-head.

A crushed zone is generated in the rock beneath a pick cutter due to the high compressive stress induced by the penetration of the pick cutter. Compressive stress induces tensile stress and tangential cracks, based on Hoop stress theory. Tensile fractures propagate to the free surface (direction of propagation is determined by minimizing fracture energy) or develop until they connect with adjacent tensile fractures. The interaction of the tensile fractures generates the rock chips. This process is the general mechanism involved in mechanical rock cutting.

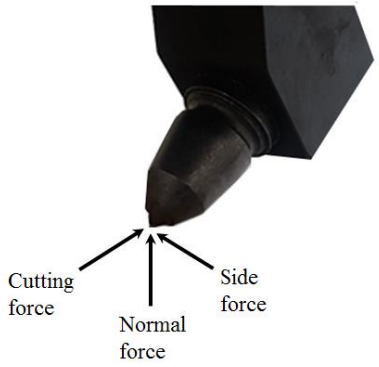

Fig. 1 Three orthogonal forces acting on a pick cutter

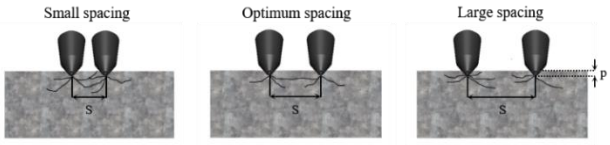

Fig. 2 Rock cutting patterns by picks according to the cut spacing (modified from Balci and Bilgin 2007)

According to this mechanism, cut spacing significantly influences the efficiency of rock cutting (Fig. 2). If the spacing between the adjacent picks is too small, no significant amount of rock chips will be formed. If the spacing is too large, no rock chips will be made at all.

*Corresponding author, Professor
E-mail: sjeon@snu.ac.kr

ISSN: 2005-307X (Print), 2092-6219 (Online)

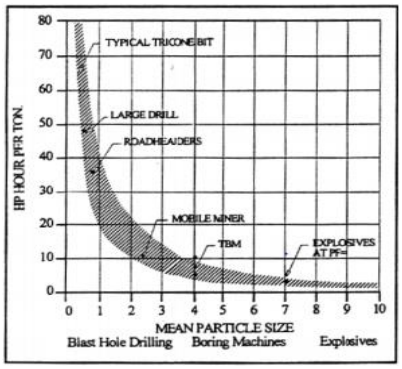

Fig. 3 Typical specific energy achieved by different mechanical excavation machine (Ozdemir 1995)

Depending on the interaction between the adjacent cutters, the cutting mode can be either relieved or unrelieved. In the relieved mode, the cutters interact (the cut spacing is small or optimum); in the unrelieved mode, no interaction occurs between the cutters (the cut spacing is too large). Thus, it is very important to determine the optimum cut spacing for a given ground condition.

Rock cutting efficiency is predominantly affected by cut spacing and the corresponding chipping behavior of the rock; therefore, the characteristics and size distribution of the rock chips produced during rock cutting process are highly related to rock cutting efficiency. The size of rock fragments produced by mechanical excavation with different cutting tools has been studied at both laboratory and field scale. The relationships between rock chip size distribution parameters, specific energy and cutter forces have been widely examined in the past studies (Ozdemir 1995, Bruland 2000, Rostami *et al.* 2002, Altindag 2003, Kahraman 2004, Tuncdemir *et al.* 2008, Farrokh and Rostami 2008).

Pfleider and Blake (1953) identified a rough correlation between penetration rate and the rock chips, and Ersoy and Waller (1997) found that the wear rate of cutter bits depends on the size of particles produced during drilling. It has since been reported that particle size is highly correlated with specific energy, which represents excavation efficiency. Ozdemir (1995) reported that specific energy drastically decreases as chip size increases (Fig. 3) and that the greater the mean chip size, the lower the specific energy and the more efficient the mechanical excavation process (Tiraky *et al.* 2010). Rostami *et al.* (2002) studied chip size and the frequency of the signal generated by rock fragmentation under a disc cutter. Bruland (2000) also carried out chip size analysis of the muck produced by TBM excavation, and described the relationships between chip size, cutter force and specific energy. Farrokh and Rostami (2008) quantitatively analyzed the size of chips in muck excavated by a TBM in fractured rock and compared the results with the thrust and torque of the TBM. Roxborough (1973) carried out a series of rock cutting experiments and revealed that values of the coarseness index (*CI*) followed a trend inverse to that of the specific energy. Higher *CI* values coincided in all cases with lower specific energy values for different operational parameters, i.e., penetration depth in rock cut by both disc cutters and chisel picks. Altindag (2003) analyzed the relationship between the size distribution parameters of rocks (namely *CI*, mean particle size and specific surface area) and the performance of percussive drilling, and found the penetration rate of percussive drilling to be highly correlated with the size distribution parameters of rock. Kahraman (2004) investigated the relationship between the *CI* of rock chips produced by top hammers and down the hole drills and the penetration rate of these machine, the results indicated that penetration rate and *CI* both decreased with drilling depth using top hammer drills. Tuncdemir *et al.* (2008) performed an LCM test using a conical pick with 17 types of rock and analyzed the correlation between cutting conditions, specific energy and the *CI*. Specific energy decreased as the *CI* increased, and the *CI* reached its maximum value at the optimum cut spacing. In addition, the *CI* increased with penetration depth.

Size distribution of rock chips obtained during the rock-cutting process can provide useful information to estimate the cutting efficiency. Chip-size distribution is should also be measured when using rock chips as aggregates and designing backup facilities for excavation machines. In addition, it is important to determine the optimum particle size for the efficient processing of mineral resources in mining engineering applications. Therefore, rock fragment size is considered of great importance to assess the efficiency of the cutting process of a mechanical excavation machine and its production during mining operations. The degree of rock fragmentation plays a significant role in controlling and minimizing the overall production cost.

However, the information is still lacking on the size distribution of the rock chips produced by rock cutting with a pick cutter and the relationship between the rock chip size distribution and the rock cutting efficiency of a pick cutter.

In this study, a series of linear cutting tests was performed to investigate the effects of cutting conditions (i.e., cut spacing and penetration depth) on the production of rock chips and their size distribution. All the rock chips produced in LCM (linear cutting machine) test were collected, and their size distribution was analyzed using a sieving test and image processing. This paper analyzes and presents the relationships between cutter force, specific energy, chip size and size-distribution parameters.

2. Experiments

2.1 LCM test

The LCM test has been proven to be an accurate and reliable method of evaluating the design parameters of a mechanical excavator. It has because two main advantages: the use of a realistic range of cutting loads and minimizing of scale effect during testing. Although the full-scale LCM test is the most reliable method of determining the design parameters of a mechanical excavator and has been applied in various cases of machine design (Roxborough and Philips 1975, Snowdon and Ryley 1982, Sanio 1985, Bilgin *et al.* 2006, Chang *et al.* 2006, Cho *et al.* 2010), it usually requires a full-size rock specimen (1000 mm×1000 mm×300 mm), which is usually difficult to obtain (Balci

and Bilgin 2007, Cho *et al.* 2013). Alternatively, a portable linear rock cutting test (Balci and Bilgin 2007, Copur 2010, Kang *et al.* 2016) can be used to predict cutting performance with small cutting tools and rock cores or small specimens. However, the use of small size specimens makes it difficult to observe the interaction between adjacent cutting grooves. In addition, the use of small-scale cutting tools makes an index test, so the test results cannot be directly used to estimate the cutting performance or to obtain the design parameters for the cutting tools.

The small-scale LCM (SLCM) system used in this study (Fig. 4) installed real size cutting tool, but the rock specimens used in the test were smaller than those used in a full-scale LCM test. Thus, the results obtained using this SLCM could be practically used to estimate cutting performance and cutting efficiency. The system had a 20 ton loading capacity and could sustain sufficient stiffness during the linear cutting tests. The system consisted of mainframe, an electronic motor unit and a control panel. The mainframe was a large stiff frame on which a conical pick was mounted.

The cutter forces were measured in three directions (normal, cutting, and side force, as shown in Fig. 1) real time, using a load cell (Fig. 5) installed between the head of the main frame and the conical pick. The rock sample was contained in a steel box to provide efficient confinement during testing. The positions of the rock specimen and the pick cutter were controlled using the control panel; in particular, the movement (cutting direction) of the rock specimen was servo-controlled to maintain a constant cutting speed. The cutting distance was also automatically controlled using the control panel to prevent the occurrence of end effects in the specimen. The cut spacing was manually controlled, and the positions of the specimen and the cutter were displayed in the control panel. The data acquisition system (Fig. 5) automatically recorded the cutting distance and cutter forces during testing.

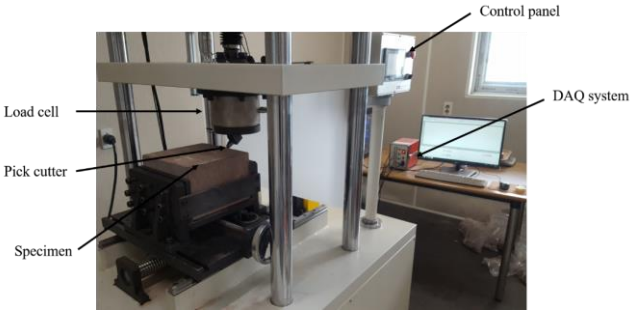

Fig. 4 Small scaled linear cutting machine system

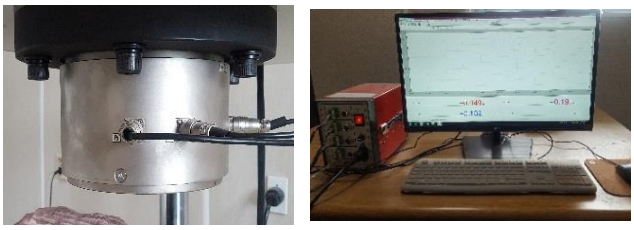

Fig. 5 A load-cell and data acquisition system to measure testing data

Table 1 Mechanical properties of Linyi sandstone

Properties	Unit	Value
Density	g/cm^3	2.4
Porosity	%	8.2
Uniaxial compressive strength	MPa	64.0
Brazilian tensile strength	MPa	4.7
Young`s modulus	GPa	10.2
Poisson`s ratio		0.2
Schmidt hammer rebound hardness*		57.3
Shore hardness*		43.5
P-wave velocity	m/s	2317
S-wave velocity	m/s	1531

*Schmidt hammer rebound and Shore hardness values were obtained by averaging the upper ten values from 20 tests performed

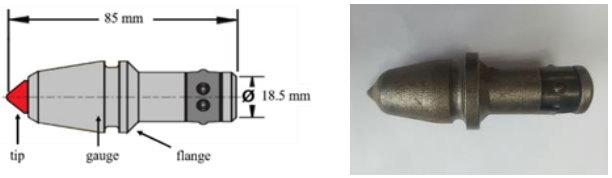

Fig. 6 A schematic drawing and photograph of a conical pick used in this study

2.2 Rock and cutting tool

The rock specimen was Linyi sandstone from China, cut into a 300 mm × 300 mm×200 mm block for testing. The mechanical properties of Linyi sandstone are presented in Table 1. They were determined using suggested testing methods by the ISRM (ISRM 2007). Linyi sandstone is considered homogeneous rock. Some sandstone is an anisotropic, to a degree dependent on its origin and characteristics. The anisotropy of rock strongly affects its strength and failure behavior (Yang *et al.* 2012). However, previous studies (Yang and Jing 2011, Kim and Jeon 2016) have shown that the degree of anisotropy of Linyi sandstone is non-significant or even negligible. Based on the literature, therefore, the potential anisotropy of the rock was assumed not to affect the test results.

The conical pick (model: PN 735MB) used in this study was manufactured by Vermeer Corporation, and its geometry is shown in the schematic drawing in Fig. 6. The cutter had a gauge of 40 mm, a primary tip angle of 70˚, a tip diameter of 12 mm, a flange diameter of 30 mm, and a shank diameter of 18.5 mm.

2.3 Testing procedure

Before a cutting test was made, the specimens were preconditioned by preliminary cutting to damage the rock surface and to replicate an actual excavated surface (Fig. 7). After preconditioning, the experiments were made under the given cutting conditions.

The testing conditions are described in Fig. 8. Penetration depth was defined as the cutting depth per pass

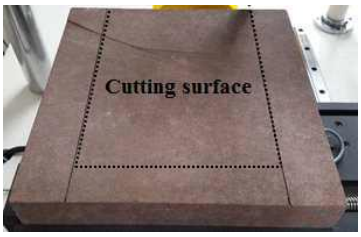

(a) Before preconditioning

(b) After preconditioning

Fig. 7 The rock specimen (a) before and (b) after preconditioning

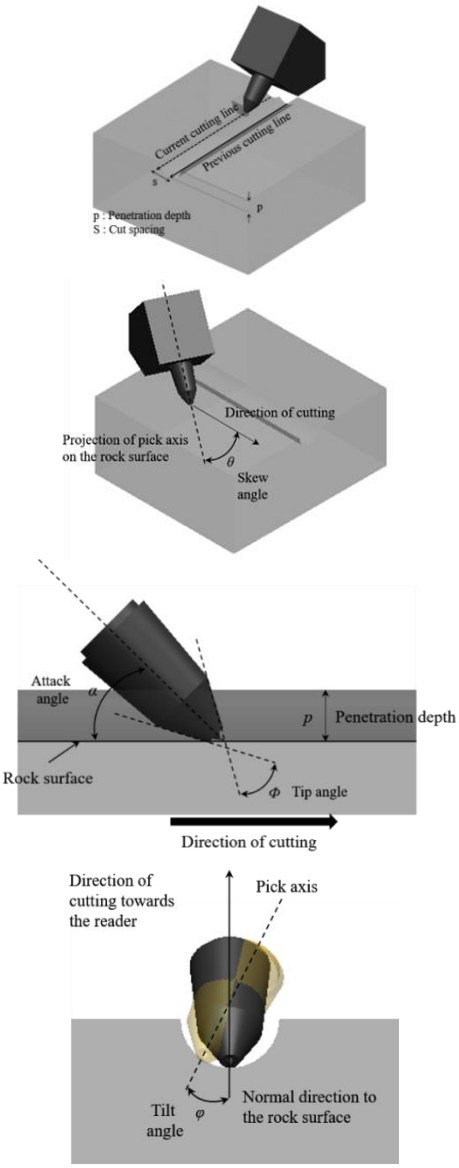

Fig. 8 Schematic diagram of testing conditions in LCM test (modified from Bilgin *et al.* 2014)

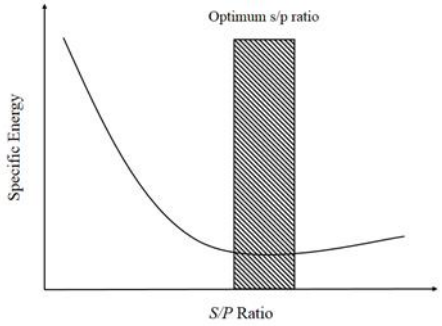

Fig. 9 Determination of the optimum cutting condition (After Cho *et al.* 2010)

of cutting; cut spacing was the spacing between adjacent cutting lines; skew angle was the minimum angle between the cutting direction and the projection of the pick axis on the rock surface; and attack angle was the angle between the pick axis and the rock surface. The skew (θ) and attack (α) angles of the pick cutter were set to 0° and 45°, respectively. The penetration depth (p) ranged from 5 mm to 11 mm, at 2 mm intervals. The s/p ratio ranged from 1 to 5, and cut spacing (s) was determined by penetration depth and the predetermined s/p ratio. The constant variables in the tests were cutting sequence (single-start) and cutting speed (10 mm/s). As previous studies have shown, the cutting speed affects neither cutter forces nor specific energy (Sanio 1985). In this study, it was assumed that the cutting speed does not affect the cutting performance of a pick cutter. The cutting distance was 200-250 mm for all cutting conditions, and at least five cutting lines were made for each case.

The cutter forces in three directions (normal, cutting and side force) were measured using a load-cell at a sampling rate of 20 s^{-1}. The forces obtained during the cutting tests were averaged to give the mean cutter forces (F_{c_mean}, F_{n_mean} and F_{s_mean}).

Specific energy is a representative index used to estimate the cutting efficiency of the mechanical cutting tools. It is defined by the work required to cut a unit volume of rock, and is calculated using Eq. (1), as follows

$$SE = \frac{F_{c\_mean} \times l}{V_{cut}} \quad (1)$$

where SE is the specific energy (unit: MJ/m^3), F_{c_mean} is the mean cutting force of a pick cutter (unit: kN), l is the cutting distance (unit: mm) and V_{cut} is the excavated rock volume (unit: m^3).

Specific energy is influenced by cut spacing; it is minimized at a specific cut spacing, namely the optimum cut spacing (or s/p ratio) (Fig. 9). The rock debris obtained in each test was collected to measure the volume of the cut rock and analyze the size distribution of the rock chips. A plastic fence was installed around the specimen box to prevent the loss of small rock particles, and the rock debris was carefully collected using a designated vacuum cleaner.

2.4 Sieve test and image processing

A sieve tester (Fig. 10) and image processing software

Fig. 10 The direct sieving tester used in this study

(a) Before (b) After

Fig. 11 Example of rock chip images before and after image processing (p = 9 mm and s = 9 mm)

Table 2 Soil particle classification

Name of organization	Grain size (mm)			
	Gravel	Sand	Silt	Clay
Unified Soil Classification (USCS)	76.2 to 4.75	4.75 to 0.075	<0.075 Fines (i.e., silts and clays)	
U.S. Department of Agriculture	>2	2 to 0.05	0.05 to 0.002	<0.002
American Association of State Highway and Transportation Officials	76.2 to 2	2 to 0.05	0.075 to 0.002	<0.002
Massachusetts Institute of Technology	>2	2 to 0.06	0.06 to 0.002	<0.002

Table 3 Example of the calculation of coarseness index

Size fraction (mm)	Retained mass (g)	Cumulative mass (%)
+19.1	73.86	16.72
-19.1 +13.2	134.07	47.06
-13.2 +9.28	76.32	64.33
-9.28 +6.56	34.02	72.03
-6.56 +4.64	32.39	79.37
-4.64 +3.28	15.84	82.95
-3.28 +2.32	9.34	85.06
-2.32 +1.64	6.62	86.56
-1.64	47.3	97.27
Total mass	429.76	CI = 631.35

were used to obtain a cumulative particle-size distribution curve. SPLIT-DESKTOP was used to analyze for the chip size distribution. The general flow of image processing was as follows. Each image acquired was cropped to separate the rock debris from the unnecessary parts, and the scale was set using the ruler in the image. The image was automatically delineated by SPLIT-DESKTOP to identify each rock chip. After the auto-delineation results were confirmed, abnormally separated or non-separated rock fragments were manually corrected. Small particles that were difficult to delineate were defined as fine material (fine factor = 5). The sieve was set at an appropriate size to enable size distribution analysis: at least larger than the biggest rock fragments so that all of the rock fragments could be analyzed. After the processing, the size distribution of the rock particles could be ascertained. Fig. 11 shows an example of images before and after processing using the software.

Countable rock chips were analyzed using image-processing software, and small particles (classified as rock powder in this study) were analyzed using the direct sieve test, because it is difficult to delineate individual small particles by image processing.

The rock fragments obtained in the cutting test were classified as either rock powder or rock chips. Many standards can be used to classify soil particles according to their size, in this study, the particles smaller than 2 mm in diameter were defined as rock powder according to the classification system (Table 2).

2.5 Determination of size distribution parameters

Many parameters describing chip size distribution are available. In soil mechanics, the coefficients of uniformity (C_u) and curvature (C_c) are normally used to represent the characteristics of particle distribution, and can be calculated by the effective sizes (D_{10}, D_{30}, and D_{60}) in the cumulative particle size distribution curve (Eqs. (2) and (3)), as follows

$$C_c = \frac{D_{60}}{D_{10}} \tag{2}$$

$$C_u = \frac{(D_{30})^2}{D_{60} \times D_{10}} \tag{3}$$

where the effective sizes D_{10}, D_{30} and D_{60} are the diameters in the particle-size distribution curve corresponding to 10%, 30%, and 60% finer, respectively. Rosin-Rammler distribution parameters also represent the distribution of rock fragments. The uniformity index (N) and the absolute size constant (D) can be defined based on the Rosin-Rammler distribution (Eq. (3)).

$$\log\left[\log\left(\frac{100}{R}\right)\right] = N \times \log(x) + D \tag{4}$$

The parameters of the Rosin-Rammler distribution, N and D are obtained from the slope of the straight line and the intercept at R = 36.79%, respectively (the substitution x = N in Eq. (3) produces a constant of about 36.79% of material retained). Together, N and D describe the size distribution of a given specimen of rock fragments subject

to sieve analysis. A small value of *N* indicates a wide size range, whereas larger values of *D* indicate that the curve is steeper and the range of sizes is narrower (Gupta and Yan 2006, Brezani and Zelenak 2010, Abu Bakar *et al.* 2014). SPLIT-DESKTOP automatically calculates these parameters based on the image-processing results and the equations described above.

Alternatively, several studies have used the *CI* to quantify the size distribution of rock debris (Roxborough and Rispin 1973, McFear-Smith and Fowell 1977, Altindag 2003, Tuncdemir *et al.* 2008, Bakar and Gerstch 2013). The *CI* is a dimensionless value calculated by summing the cumulative weight percentages retained on each sieve used. It is dependent on and thus changes with the sieve size, so it changes according to the sieve size. Thus, the *CI* can be used to compare the characteristics of rock particles sieved using the same set of sieves. In this study, the maximum and minimum sieve diameters were 19.1 mm and 1.64 mm, respectively. Table 3 shows representative results for the *CI*.

3. Results

3.1 Cutter force and specific energy

The cutter forces and specific energy under different cutting conditions are summarized in Table 4. The mean cutter forces are the averaged values of the forces obtained in the tests. Fig. 12 shows the relationships between the mean cutter forces and the *s/p* ratio. The normal and cutting forces linearly increased with cut spacing at all penetration depths, and the cutter forces also increased with penetration depth.

Table 4 The result of cutting force and specific energy in different cutting conditions

p (mm)	*s* (mm)	*s/p*	Mean cutter force, F_{mean} (kN)			Specific energy (MJ/m^3)
			Side	Cutting	Normal	
5	5	1	0.81	3.21	3.61	82.96
	10	2	0.13	4.25	4.38	77.65
	15	3	0.17	5.21	5.29	77.86
	20	4	0.53	5.81	5.87	67.57
	25	5	0.27	6.32	6.43	85.81
7	7	1	0.47	3.48	3.51	54.74
	14	2	0.54	5.08	5.13	48.94
	21	3	0.61	6.07	6.84	42.17
	28	4	0.84	6.96	7.25	44.94
9	9	1	0.60	5.02	5.65	49.73
	13.5	1.5	0.51	6.15	7.20	45.66
	18	2	0.52	6.63	7.96	37.69
	22.5	2.5	0.39	8.29	9.18	36.50
	27	3	0.52	7.59	9.40	33.12
	36	4	0.78	8.30	10.95	39.70
11	11	1	0.26	6.97	7.29	46.30
	22	2	0.63	7.93	8.39	34.39
	33	3	1.27	8.90	9.64	31.10
	44	4	1.30	10.02	12.96	32.71

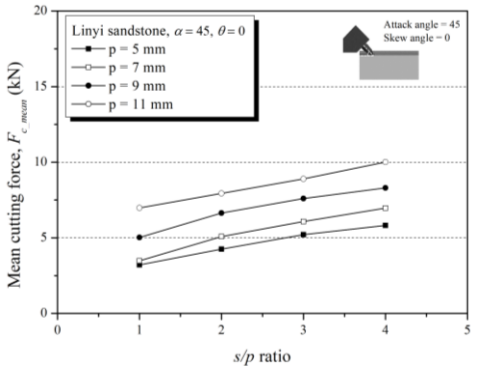

(a) Cutting force

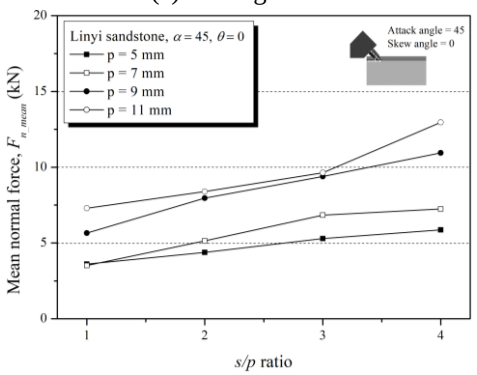

(b) Normal force

Fig. 12 The relationship between the cutter forces and cutting conditions

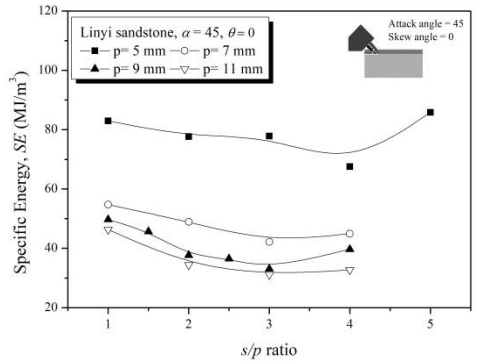

Fig. 13 Variation of specific energy depending on the cutting conditions

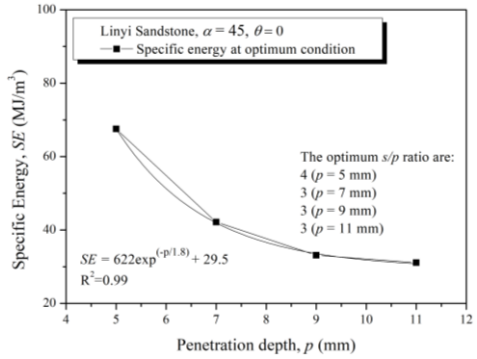

Fig. 14 The relationship between the penetration depth and the specific energy at the optimum cutting condition

Fig. 13 shows the relationship between cut spacing and

specific energy. The optimum cutting condition was defined as the optimum *s/p* ratio at the minimum specific energy. The optimum *s/p* ratio at the 5 mm penetration depth was 4, and the optimum *s/p* ratio at the other penetration depths was 3 (see Fig. 13). The optimum *s/p* ratio decreased as penetration depth increased. Fig. 14 shows the relationship between penetration depth and specific energy at the optimum cut spacing. The specific energy at the optimum cutting condition decreased in exponentially with penetration depth, which ranged from 5 mm to 11 mm. Although the range of penetration depths considered was limited, the result indicated that when penetration depth is deeper, a smaller *s/p* ratio should be established for more efficient cutting. In addition, specific energy decreased with increasing penetration depth. Thus, machine operation was optimized at a large penetration depth per revolution (per cutting pass for each cutter), dependent on the machine`s capacity (thrust and torque). Previous researchers (Chang *et al.* 2006, Cho 2010) reported the concept of the "*optimum penetration depth*." defined as the specific penetration depth yielding a minimum (or converged) specific energy. In this study, the optimum penetration depth was not clearly defined, due to a lack of data for higher values of penetration depth; based on the trend line, however, it was expected to occur at 11 mm or more in penetration depth.

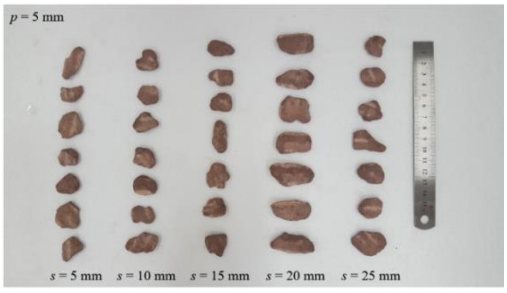

(a) p = 5 mm

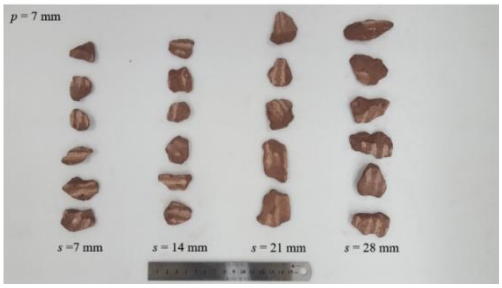

(b) p = 7 mm

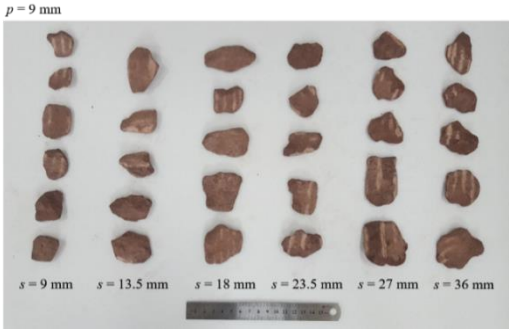

(c) p = 9 mm

Fig. 15 Photographs of the rock chips at the different penetration depths and cut spacings

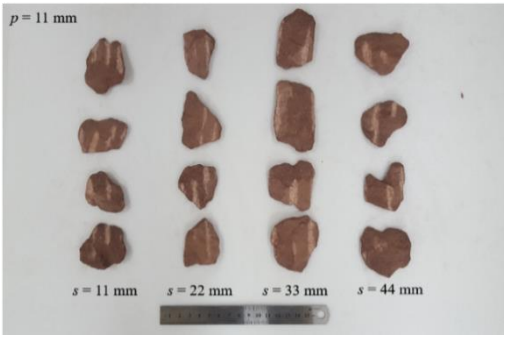

(d) p = 11 mm

Fig. 15 Continued

Table 5 The results of chip size and distribution in different cutting conditions

Cutting conditions (mm)		Distribution parameters				Particle size (mm)					
p	*s*	C_u	C_c	*CI*	*N*	*D*	D_{10}	D_{30}	D_{50}	D_{60}	D_{max}
5	5	3.94	1.37	521.49	1.60	11.85	2.93	6.81	10.06	11.54	26.68
	10	3.16	1.29	527.47	1.86	11.49	3.55	7.16	9.88	11.23	24.39
	15	3.43	1.34	562.34	1.85	12.33	3.80	8.16	11.46	13.04	27.21
	20	4.90	1.44	575.22	1.42	14.75	3.02	8.01	12.61	14.79	35.51
	25	4.10	1.38	561.64	1.54	13.75	3.24	7.71	11.49	13.29	37.56
7	7	5.81	1.49	557.61	1.32	13.84	2.42	7.11	11.76	14.05	41.07
	14	4.08	1.3	660.01	1.47	20.22	4.55	10.49	15.66	18.55	49.30
	21	3.02	1.27	659.19	1.92	17.62	5.90	11.57	15.74	17.82	38.68
	28	4.01	1.38	669.76	1.57	19.74	4.98	11.69	17.38	19.95	46.4
9	9	3.74	1.35	654.86	1.71	17.52	4.99	11.21	16.31	18.64	38.70
	13.5	4.46	1.33	699.34	1.41	23.69	5.08	12.37	18.93	22.64	52.81
	18	3.87	1.37	728.87	1.51	25.95	6.25	14.39	21.06	24.21	53.21
	23.5	3.49	1.34	696.50	1.72	20.85	6.14	13.26	18.85	21.4	40.95
	27	3.83	1.36	736.24	1.56	25.32	6.45	14.69	21.50	24.69	61.76
	36	3.59	1.34	734.23	1.62	25.41	6.86	15.07	21.74	24.66	50.22
11	11	15.26	1.84	670.99	0.90	25.10	1.74	9.23	20.30	26.55	66.35
	22	4.09	1.38	708.39	1.49	23.78	5.62	13.35	19.96	23.00	50.94
	33	7.67	1.61	755.99	1.16	28.55	4.10	14.41	25.77	31.44	77.77
	44	4.99	1.44	714.97	1.33	25.93	5.02	13.44	21.43	25.07	53.72

3.2 Chip size and distribution

In this study, all of the rock chips generated in a series of linear cutting tests were collected to analyze their size distribution, as mentioned above. Fig. 15 shows the rock chips collected at different penetration depths and cut spacings. Fig. 16 shows representative chips with optimum cut spacing (defined in Fig. 13) at different penetration depths.

As the cut spacing increased, the size of the rock chips also gradually increased, reaching it maximum value at the optimum cut spacing. The maximum chip size was obtained at the penetration depth of 11 mm and the cut spacing of 33 mm. After the optimum cut spacing for each depth. Such as 25 mm of cut spacing at 5 mm penetration depth, chip size

Table 6 The spearman correlation matrix of the parameters

	Cutting conditions		LCM results			Distribution parameters				Particle size					
	p	s	F_{c_mean}	F_{n_mean}	SE^*	C_u	C_c	CI	N	D	D_{10}	D_{30}	D_{50}	D_{60}	D_{max}
p		0.38	0.81	0.83	0.83	0.37	0.34	0.82	-0.48	0.87	0.42	0.73	0.88	0.92	0.88
s			0.81	0.79	-0.25	0.04	0.16	0.68	-0.05	0.60	0.54	0.73	0.64	0.56	0.44
F_{c_mean}				0.98	-0.66	0.25	0.34	0.85	-0.30	0.84	0.54	0.83	0.87	0.86	0.74
F_{n_mean}					-0.69	0.26	0.29	0.86	-0.31	0.85	0.54	0.83	0.86	0.87	0.76
SE						-0.17	-0.09	-0.76	0.32	-0.78	-0.53	-0.69	-0.76	-0.79	-0.74
C_u							0.82	0.71	-0.97	0.32	-0.48	-0.05	0.27	0.40	0.53
C_c								0.15	-0.74	0.28	-0.46	-0.02	0.28	0.38	0.41
CI									-0.32	0.96	0.70	0.96	0.97	0.93	0.87
N										-0.47	0.34	-0.10	-0.40	-0.52	-0.66
D											0.58	0.89	0.97	0.96	0.93
D_{10}												0.84	0.60	0.46	0.35
D_{30}													0.92	0.83	0.74
D_{50}														0.97	0.90
D_{60}															0.95
D_{max}															

*SE is specific energy

Fig. 16 Representative rock chips in different penetration depth at optimum cut spacing

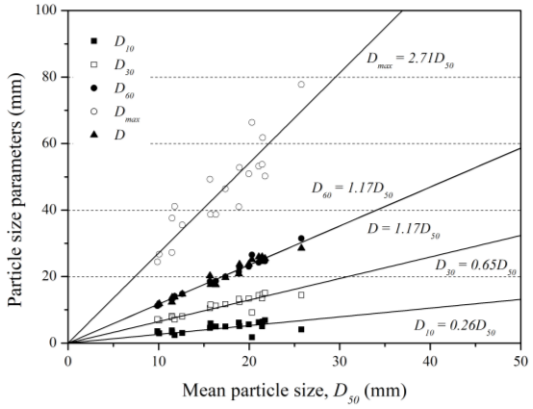

Fig. 17 The relationship between the mean particle size and the different particle size parameters

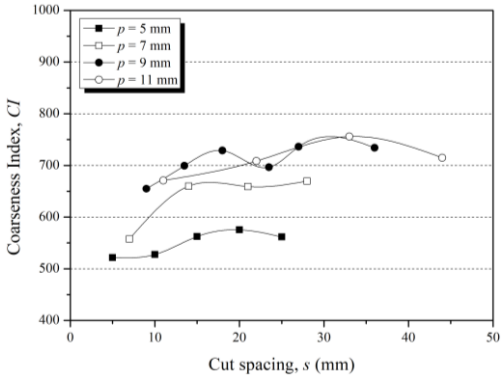

(a) Cut spacing

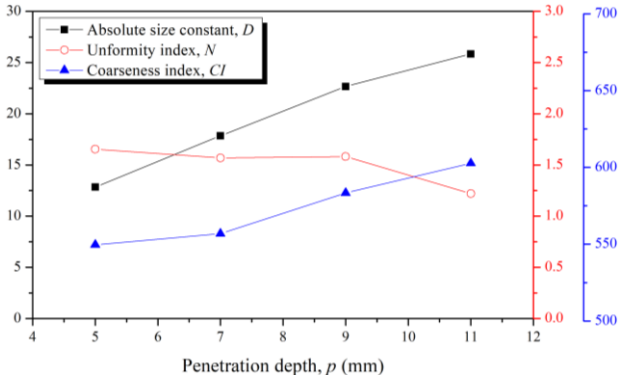

(b) Penetration depth

Fig. 18 The relationship between chip size distribution parameter (a) cut spacing and (b) penetration depth

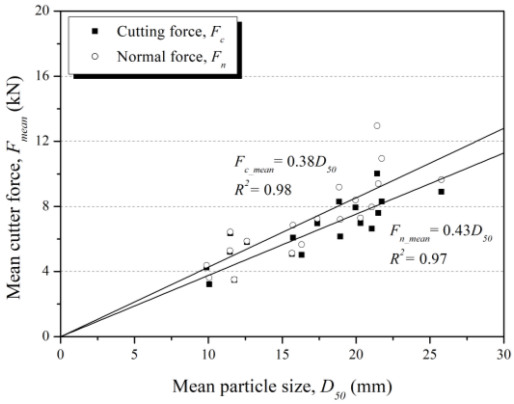

(a) Cutter force

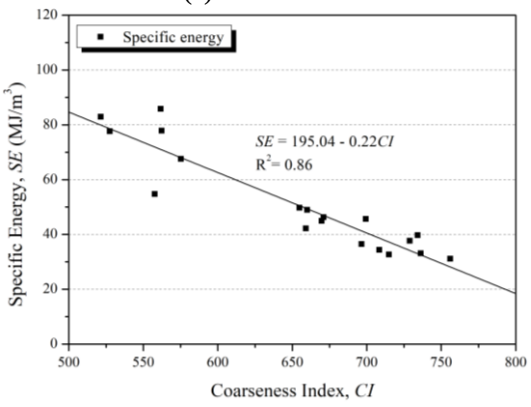

(b) Specific energy

Fig. 19 The relationship between chip size distribution parameters, (a) cutter force and (b) specific energy

decreased or became consistent. The representative sizes of the rock chips at each penetration depth were 20 mm × 35 mm, 27 mm × 45 mm, 35 mm × 55 mm and 75 mm × 45 mm, respectively. As the cut spacing increased, the size of the rock chips also gradually increased. The rock chips were largest at the optimum cut spacing. The maximum chip size appeared at the 11 mm of penetration depth and 33 mm of cut spacing.

Table 5 presents the results of chip size and size distribution. The relationship between these variables was analyzed using the Spearman correlation matrix as summarized in Table 6.

Of the parameters under this study, determined by different methods, the coefficients of uniformity (C_u) and the uniformity index (N) were highly correlated with each other (r = -0.97). The absolute size constant (D) showed a good correlation with D_{30}, D_{50}, D_{60} and D_{max}; however, it correlated poorly with D_{10}. The results thus suggested that the N and D values determined using the Rosin-Rammler distribution can provide more representative information on the particle size and size distribution of the rock chips, respectively, than the parameters based on soil mechanics can. The CI was highly correlated with D, D_{30}, D_{50}, and D_{60} (r = 0.96, 0.96, 0.97 and 0.93, respectively), the cutter forces and the specific energy. However, it correlated poorly with the size distribution parameters. The CI can thus be considered to represent particle size rather than size distribution. Fig. 17 shows the relationship between the mean particle size (D_{50}) and the particle size parameters at different passing rates (10%, 30%, 60% and 100%). The particle sizes at different passing rates had good linear relationships with the mean particle size. However, D_{10} showed less correlation with the mean particle size, based on Spearman correlation analysis. The maximum particle size (D_{max}) was 2.7 times greater than the mean particle size. As a result, the mean particle size can be considered the parameter most representative of particle size when the passing rate is greater than 30%.

Fig. 18 (a) shows the effect of cut spacing on particle size represented by CI. The CI tended to reach its maximum value at the optimum cut spacing for each penetration depths. Fig. 18 (b) shows the effects of penetration depth on the characteristics of particle size and size distribution. It is clear that the larger penetration depth, the larger the rock chips produced, and the less uniform their size distribution. In addition, particle size and size distribution were found to be more dependent on penetration depth than on the cut spacing. Rock cutting theory has shown that maximizing rock fragmentation results in the most efficient rock-cutting. Similarly, the results of this study indicated that operational conditions with deep penetration depth resulted in efficient cutting. Fig. 19(a) shows the relationship between the cutter forces and mean particle size (D_{50}). Two cutter forces (normal and cutting) linearly increased with the mean particle size. This indicates that larger cutter forces were required to cut the rock into larger debris. Fig. 19(b) shows the relationship between the CI and specific energy. A larger CI indicates that the cutting is more efficient.

3.3 Rock powder generation

Efficient rock-cutting is well known to maximize chip size. During rock cutting, compressive stress concentration occurs directly under the cutter in contact with the rock, crushing the rock in that part into rock powder (very fine material) rather than rock chips. It is not desirable to increase the proportion of rock powder in the areas mined by mechanical excavation, because rock powder is more difficult to recover than rock chips. In subsea conditions, in

Table 6 The results of rock powder generation in different cutting conditions

Cutting conditions (mm)		Total rock debris	Remained rock debris on sieve (g)				Chip (g)	Powder (g)	Powder/ Chip (%)	Powder/ Total (%)
p	*s*	(g)	#20	#40	#100	#200				
5	5	220.8	154.0	24.1	32.7	10.0	154.0	66.8	43.4	30.3
	10	316.8	225.9	31.3	47.0	12.6	225.9	90.9	40.2	28.7
	15	189.7	138.7	18.4	22.2	10.4	138.7	51.0	36.8	26.9
	20	246.8	181.5	23.2	33.4	8.7	181.5	65.3	36.0	26.5
	25	210.8	151.8	19.6	26.9	12.5	151.8	59.0	38.9	28.0
7	7	164.2	122.2	15.9	16.2	9.9	122.2	42.0	34.4	25.6
	14	275.2	209.7	22.7	25.5	17.3	209.7	65.5	31.2	23.8
	21	367.9	287.9	27.2	30.7	22.1	287.9	80.0	27.8	21.8
	28	416.0	327.3	39.3	35.9	13.5	327.3	88.7	27.1	21.3
9	9	352.0	281.8	23.9	32.4	13.9	281.8	70.2	24.9	20.0
	13.5	440.9	371.0	23.2	31.9	14.8	371.0	69.9	18.8	15.8
	18	516.4	414.4	11.7	50.3	40.0	414.4	102	24.6	19.8
	23.5	424.7	359.7	24.4	23.2	17.4	359.7	65.0	18.1	15.3
	27	468.1	420.4	21.0	23.5	3.2	420.4	47.7	11.4	10.2
	36	365.0	311.7	22.7	20.4	10.2	311.7	53.3	17.1	14.6
11	11	306.5	266.8	17.3	15.2	7.2	266.8	39.7	14.9	13.0
	22	475.7	425.0	21.0	20.6	9.1	425.0	50.7	11.9	10.7
	33	593.0	536.9	24.0	21.8	10.3	536.9	56.1	10.5	9.5
	44	473.5	427.3	20.4	17.0	8.8	427.3	46.2	10.8	9.8

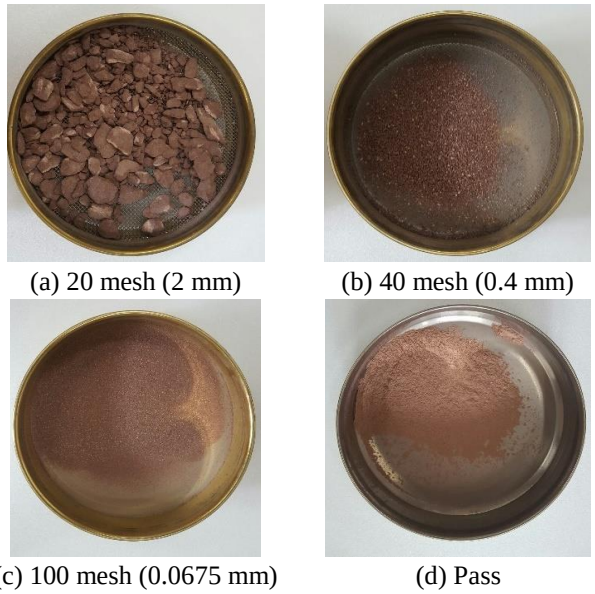

(a) 20 mesh (2 mm) (b) 40 mesh (0.4 mm)

(c) 100 mesh (0.0675 mm) (d) Pass

Fig. 20 The rock particles sieved by the 20, 40 and 100 meshes of standard sieves

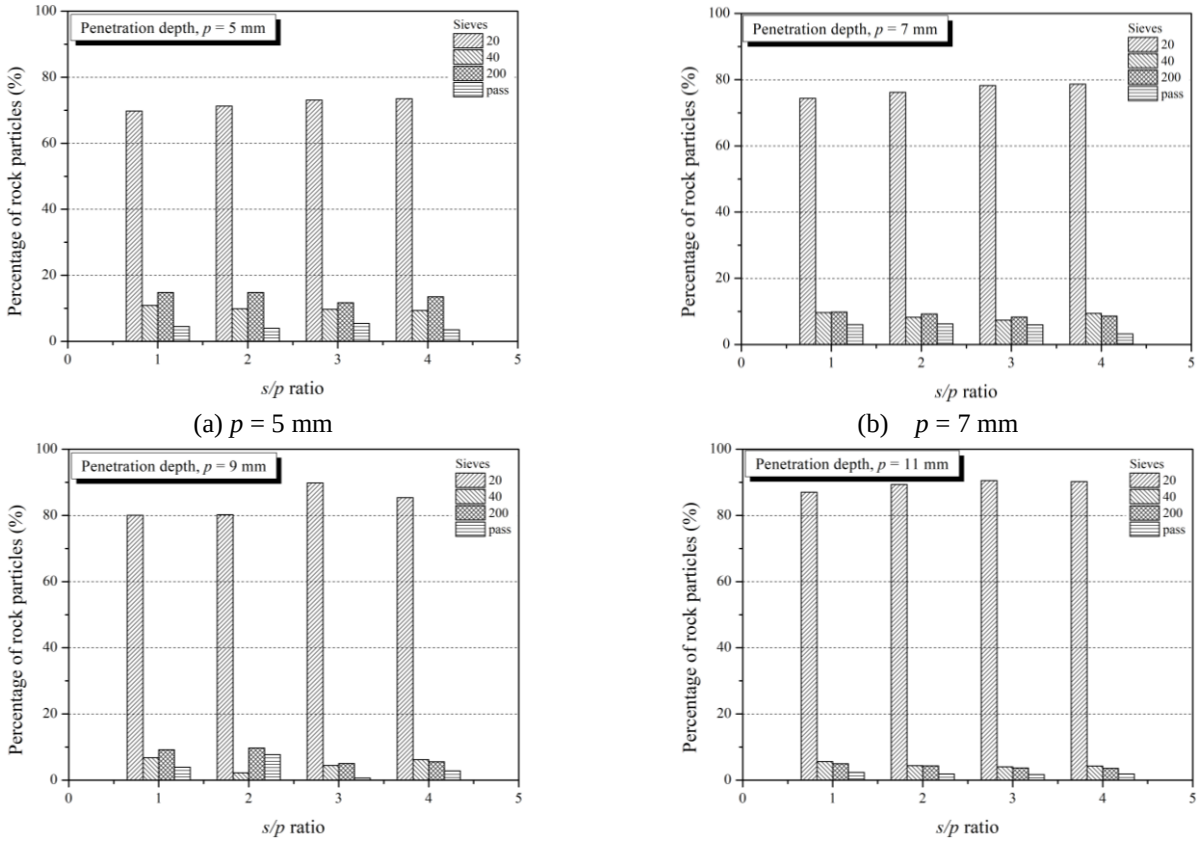

(a) p = 5 mm (b) p = 7 mm

(c) p = 9 mm (d) p = 11 mm

Fig. 21 The distribution of the sieved rock particles according to the penetration depth and cut spacing

particular, rock powder forms a slurry in water, which increases the cutter force required and reduces the cutting efficiency (Jackson *et al.*, 2007).

Table 6 presents the results of the rock powder analysis. Fig. 20 shows the rock particles sieved in each sieve (as mentioned in Section 2.4), and Fig. 21 shows the distribution of the rock particles sieved in #20 (2 mm), #40 (0.4 mm) and #200 (0.0675 mm) mesh standard sieves according to cut spacing and penetration depth.

The results indicated that the proportions of the rock particles sieved by each sieve (with respect to the total mass) were consistent with cut spacing. As shown in Fig. 21, the average proportions of rock powder in the total weight of cut rock at the penetration depths of 5 mm, 7 mm, 9 mm and 11 mm were 28.1% (26.5%~30.3%), 23.1% (21.3%~25.6%), 15.9% (10.2%~19.9%) and 11.5% (9.5%~13.0%), respectively. In addition, the percentages of rock powder for significant chips at the penetration depths of 5 mm, 7 mm, 9 mm and 11 mm were 39.5% (36.0%~43.4%), 30.1% (27.1%~34.37%), 19.2% (11.4%~24.9%) and 12.0% (10.5%~14.9%), respectively.

The proportion of rock powder tended to decrease linearly with penetration depth (Fig. 22). This result is unsurprising as the likelihood of producing a large chip increases with penetration depth. As the penetration depth changes, the size and shape of the cross-sectional area between the rock and pick will also change, and these changes affect the friction between the rock and the pick cutter and the shape and area of the stress field in the

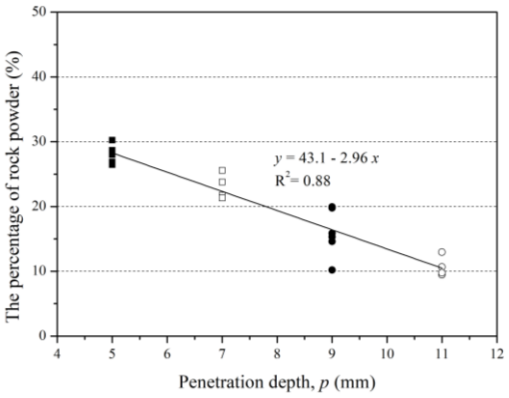

Fig. 22 The rock powder proportion according to the penetration depth

crushed zone. This was evident from the results of rock powder ratio analysis, and confirming that penetration depth greatly affects the efficiency of the rock cutting. Cut spacing also affected the proportion of rock powder, which was minimized at the optimum cut spacing. However, the effect of cut spacing on the proportion of rock powder was smaller than that of penetration depth.

As rock chips are created by the interaction between cracks formed by adjacent cutters, the larger the mass of the chipped rock and the larger the chip size, the more efficient the cutting. In contrast, rock powder is produced by the high level of compressive stress in the crushed zone. Therefore, the proportion of rock powder in the total volume of cut

rock is another indicator of cutting efficiency. The larger the proportion of rock powder, the more inefficient the cutting.

4. Conclusions

In this study, a series of linear cutting test was performed to investigate the effect of cutting conditions (specifically cut spacing and penetration depth) on the production the size distribution of rock chips. Penetration depth is a very important parameter influencing rock chip size and size distribution during the rock cutting process. The size of rock chips was found to significantly increase with penetration depth. Cut spacing is well known to be the main determinant of chipping behavior during rock cutting process. The results for size distribution and particle size also showed that the optimum cut spacing made the maximum size of rock chips, and indicating efficient rock cutting. The relationships between the chip size distribution parameters, cutter forces and specific energy were investigated using image processing and sieving analysis. The cutter force were observed to increase with rock chip size. The *CI*, mean particle size and the absolute size constant were also found to be highly correlated with the specific energy. The results of statistical supported the experimental observations. As the size and size distribution of rock chips produced by rock cutting directly reflect rock cutting efficiency, rock chip size can be used as an index of cutting efficiency. It will be necessary to build a database of experimental results and field practices with more rock types and cutting conditions. In addition, image processing was found to provide the quantitative information required to analyze the size distribution of rock chips, whereas rock powder as best analyzed using the direct sieve test.

The proportion of rock powder (diameter less than 2 mm) in the total volume of cut rock was analyzed. The amount of rock powder in the crushed zone was highly correlated with the specific energy. The proportion of rock powder was also found to exceed 20% at the considered cutting conditions under study. The results showed that the ratio of rock powder to the cutting volume fell between 20% and 50% depending on penetration depth and cut spacing. The ratio was reduced by increasing the penetration depth. The results of this study can be used to optimize cutting efficiency and to determine the optimum particle size for the efficient processing of mineral resources in mining engineering application.

However, the results of this study and the conclusions drawn from them were based on a limited range of rock type and cutting tool. As the characteristics of rock fragmentation during rock cutting are obviously influenced by rock type and cutting tool, added testing is required to better understand this relationship. In addition, further research on the effects of skew angle, attack angle and cutting speed on size distribution of rock chips is in demand.

Acknowledgements

This study was funded by the Korea Agency for Infrastructure Technology Advancement under the Ministry of Land, Infrastructure and Transport in Korea (Project No. : 13CCTI-T01).

References

Altindag, R. (2003), "Estimation of penetration rate in percussive drilling by means of coarseness index and mean particle size", *Rock Mech. Rock Eng.*, **36**(4), 323-332.

Abu Bakar, M.Z. and Gertsch, L.S. (2013), "Evaluation of saturation effects on drag pick cutting of a brittle sandstone from full scale linear cutting tests", *Tunn. Undergr. Sp. Technol.*, **34**, 124-134.

Abu Bakar, M.Z., Gertsch, L.S. and Rostami, J. (2014), "Evaluation of fragments from disc cutting of dry and saturated sandstone", *Rock Mech. Rock Eng.*, **47**(5), 1891-1903.

Balci, C. and Bilgin, N. (2007), "Correlative study of linear small and full-scale rock cutting tests to select mechanized excavation machines", *J. Rock Mech. Min. Sci.*, **44**(3), 468-476.

Bilgin, N., Demircin, M.A., Copur, H., Balci, C., Tuncdemir, H. and Akcin, N. (2006), "Dominant rock properties affecting the performance of conical picks and the comparison of some experimental and theoretical results", *J. Rock Mech. Min. Sci.*, **4**(1), 139-156.

Brezani, I. and Zelenak, F. (2010), "Improving the effectivity of work with Rosin-Rammler diagram by using MATLAB GUI tool", *Acta Montanistica Slovaca*, **15**(2), 152-157.

Bruland, A. (2000), "Hard rock performance data and back-mapping", Ph.D. Dissertation, Norwegian University of Science and Technology, Trondheim, Norway.

Copur, H, (2010), "Linear stone cutting tests with chisel tools for identification of cutting principles and predicting performance of chain saw machines", *J. Rock Mech. Min. Sci.*, **47**(1), 104-120.

Chang, S.H., Choi, S.W., Bae, G.J. and Jeon, S. (2006), "Performance prediction of TBM disc cutting on granitic rock by the linear cutting test", *Tunn. Undergr. Sp. Technol.*, **21**(3-4), 271.

Chang, S.H., Lee, C.H., Kang, T.H., Ha, T.W. and Choi, S.W. (2017), "Effect of hardening on wear reduction of pick cutters under mixed rock conditions", *Geomech. Eng.*, **13**(1), 141-159.

Cho, J.W., Jeon, S.W., Yu, S.H. and Chang, S.H. (2010), "Optimum cut spacing of TBM disc cutters: A numerical simulation using the three0dimensional dynamic fracturing method", *Tunn. Undergr. Sp. Technol.*, **25**(3), 230-244.

Cho, J.W., Jeon, S., Jeong, H.Y. and Chang, S.H. (2013), "Evaluation of cutting efficiency during TBM cutter excavation within Korean granitic rock using linear cutting machine testing and photogrammetric measurement", *Tunn. Undergr. Sp. Technol.*, **35**, 37-54.

Ersoy, A. and Waller, M.D. (1997), "Drilling detritus and the operating parameters of thermally stable PDC core bits", *J. Rock Mech. Min. Sci.*, **34**(7), 1109-1123.

Farrokh, E. and Rostami, J. (2008), "Correlation of tunnel convergence with TBM operational parameters and chip size in the Ghomroud tunnel, Iran", *Tunn. Undergr. Sp. Technol.*, **23**(6), 700-710.

Gupta, A. and Yan, D. (2006), *Mineral Processing Design and Operation*, Elsevier Science, Amsterdam, The Netherlands.

ISRM (2007), *The Complete ISRM Suggested Methods for Rock Characterization, Testing and Monitoring: 1974-2006*, in *The Blue Book*, International Society for Rock Mechanics, Commission on Testing Methods.

Jackson, E. and Devaux, M. (2007), "Performance prediction for a subsea mechanical trenching wheel", *Proceedings of the 6th*

International Offshore Site Investigation and Geotechnics, Confronting New Challenges and Sharing Knowledge, London, U.K., September.

Jeong, H.Y., Lee, S.D. and Jeon, S.W. (2014), "Current and future study on assessment of cutting performance of hard rock TBM in Korea", *Proceedings of the 14th World Conference of the Associated research Centers for the Urban Underground Space (ACUUS 2014)*, Seoul, Korea, September.

Jeong, H.Y., Cho, J.W., Jeon, S.W. and Rostami, J. (2016), "Performance assessment of hard rock TBM and rock boreability using punch penetration test", *Rock Mech. Rock Eng.*, **49**(4), 1517-1532.

Kahraman, S., Develi, K. and Yasar, E. (2004), "Predicting the penetration rate of percussive blast hole drills using coarseness index and median particle size", *CIM Bull.*, **97**, 1083.

Kang, H., Cho, J.W., Park, J.Y., Jang, J.S., Kim, J.H., Kim, K.W., Rostami, J., Lee, J.W. (2016), "A new linear cutting machine for assessing the rock-cutting performance of a pick cutter", *J. Rock Mech. Min. Sci.*, **88**, 129-136

Kim, T.H. and Jeon, S.W. (2016), "A study on shear characteristics of a rock discontinuity under various thermal, hydraulic and mechanical conditions", *Tunn. Undergr. Sp. Technol.*, **26**(2), 749-755.

McFeat-Smith, I. and Fowell, R.J. (1977), "Correlation of rock properties and the cutting performance of tunnelling machines", *Proceedings of the Conference on Rock Engineering*, Newcastle Upon Tyne, England.

Ozdemir, L. (1995), "No-dig engineering", *Trenchless Technol.*, **2**(1), 18.

Pfleider, E.P. and Blake, R.L. (1953), "Research on the cutting action of the diamond drill bit", *Min. Eng.*, **5**, 187-195.

Rostami, J., Gerstsch, R. and Gertsch, L. (2002), "Rock fragmentation by disc cutter a critical review and an update", *Proceedings of the North American Rock Mechanics Symposium (NARMS)-Tunneling Association of Canada (TAC) Meeting*, Toronto, Canada, July.

Roxborough, F.F. and Rispin, A. (1973), "A laboratory investigation into the application of picks for mechanized tunnel boring in the lower chalk", *Min. Eng.*, **133**(1), 13.

Sanio, H.P. (1985), "Prediction of the performance of disc cutters in anisotropic rock", *J. Rock Mech. Min. Sci. Geomech. Abstr.*, **22**(3), 153-161.

Snowdon, R.A., Ryley, M.D. and Temporal, J. (1982), "A study of disc cutting in selected British rocks", *J. Rock Mech. Min. Sci. Geomech. Abstr.*, **19**(3), 107-121.

Tiryaki, B., D. Gipps, I. and Li, X. (2010), *Laboratory Comparision of Mini-Discs with Point Attack Picks*, in *Advanced Materials Research*, Trans Tech Publications, 189-194.

Tuncdemir, H., Bilgin, N., Copur, H. and Balci, C. (2008), "Control of rock cutting efficiency by muck size", *J. Rock Mech. Min. Sci.*, **45**(2), 278-288.

Yang, S.Q. and Jing, H.W. (2011), "Strength failure and crack coalescence behavior of brittle sandstone samples containing a single fissure under uniaxial compression", *J. Fract.*, **168**(2), 227-250.

Yang, X.Q., Zhang, L.J. and Ji, X.M. (2013), "Strength characteristics of transversely isotropic rock materials", *Geomech. Eng.*, **5**(1), 71-86.

CC